Nuclear Engineering and Technology 52 (2020) 461–468

Contents lists available at ScienceDirect

Nuclear Engineering and Technology

journal homepage: www.elsevier.com/locate/net

Original Article

Improvement and application of DeCART/MUSAD for uncertainty analysis of HTGR neutronic parameters

Tae Young Han [a], Hyun Chul Lee [b, *], Jin Young Cho [a], Chang Keun Jo [a]

[a] Korea Atomic Energy Research Institute, 111 Daedeok-daero, 989beon-gil, Yuseong-gu, Daejeon, 305-353, South Korea
[b] Pusan National University, 2 Busandaehak-ro 63beon-gil, Geumjeong-gu, Busan, 609-735, South Korea

ARTICLE INFO

Article history:
Received 15 April 2019
Received in revised form
11 July 2019
Accepted 9 August 2019
Available online 10 August 2019

Keywords:
Uncertainty
Generalized perturbation theory
Double heterogeneity
MUSAD
DeCART

ABSTRACT

The improvements of the DeCART/MUSAD code system for uncertainty analysis of HTGR neutronic parameters are presented in this paper. The function for quantifying an uncertainty of critical-spectrum-weighted few group cross section was implemented using the generalized adjoint B_1 equation solver. Though the changes between the infinite and critical spectra cause a considerable difference in the contribution by the graphite scattering cross section, it does not significantly affect the total uncertainty. To reduce the number of iterations of the generalized adjoint transport equation solver, the generalized adjoint B_1 solution was used as the initial value for it and the number of iterations decreased to 50%. To reflect the implicit uncertainty, the correction factor was derived with the resonance integral. Moreover, an additional correction factor for the double heterogeneity was derived with the effective cross section of the DH region and it reduces the difference from the complete uncertainty. The code system was examined with the MHTGR-350 Ex.II-2 3D core benchmark. The k_{eff} uncertainty for Ex.II-2a with only the fresh fuel block was similar to that of the block and the uncertainty for Ex.II-2b with the fresh fuel and the burnt fuel blocks was smaller than that of the fresh fuel block.

1. Introduction

For an uncertainty analysis of a high temperature gas-cooled reactor (HTGR), the MUSAD (Modules of Uncertainty and Sensitivity Analysis for DeCART) [1,2] code has been developed based on the generalized perturbation theory (GPT) [3,4]. The code is used in the lattice physics analysis step of the two-step uncertainty analysis procedure [5,6]. It can provide sensitivities and uncertainties for general responses with the generalized adjoint fluxes calculated by the DeCART code [7] and also generates randomly sampled few-group cross section sets for the CAPP code [8], which is a core simulation code for block type HTGR cores.

The DeCART code can directly solve the generalized adjoint equation for the double heterogeneity (DH) region which is composed of the graphite matrix and TRISO fuel particles randomly dispersed in the matrix. For this, two generalized adjoint equation solvers were implemented into the DeCART code [2]. The first one is the generalized adjoint transport equation solver extended for the DH problems based on the Sanchez-Pomraning method [9] which was implemented in the forward transport equation solver of the DeCART [10]. The second one is the generalized adjoint B_1 equation solver which provides the generalized adjoint flux in one homogenized problem region without a spatial dependency or explicit DH treatment.

The aim of this paper is to present recent improvements of the DeCART/MUSAD code system for the uncertainty analysis of HTGR neutronic parameters. First, the function for quantifying an uncertainty of a critical-spectrum-weighted few group cross section was implemented using the generalized adjoint B_1 equation solver. In the lattice physics analysis step of the two-step uncertainty analysis procedure, a cross section uncertainty provided by DeCART/MUSAD was usually calculated with an infinite spectrum of a fuel block or assembly. Actually, few-group cross sections for a nuclear design should be generated with a critical spectrum weighting. Therefore, it is necessary to evaluate the difference between the few-group cross section uncertainties with the infinite spectrum and critical spectrum. The second is the improvement of the convergence for the generalized adjoint transport equation solver. The coarse mesh finite difference (CMFD) acceleration cannot be used for the method of characteristics (MOC) iteration in the generalized adjoint transport equation solver. Thus, it has a slow convergence by MOC-only iterations. To improve this, the generalized adjoint B_1 solution

* Corresponding author.
E-mail address: hyunchul.lee@pusan.ac.kr (H.C. Lee).

https://doi.org/10.1016/j.net.2019.08.006

can be used as the initial value for the generalized adjoint transport solution. The third improvement is to apply the correction factor for the implicit uncertainty reflecting the resonance self-shielding effect and the DH effect. The correction factor is derived with the resonance integral and the effective cross section used in DeCART.

The methodologies and the verification results for the three improvements are described in Sections 2 and 3. In addition, the DeCART/MUSAD code system was applied to an uncertainty analysis of the MHTGR-350 Ex.II-2 3D core benchmark proposed by the IAEA CRP for the HTGR uncertainty analysis in modeling (UAM) [11], and the analysis results are provided in Section 4.

2. Application of the generalized adjoint B_1 equation

DeCART has two generalized adjoint equation solvers: the generalized adjoint transport equation solver and the generalized adjoint B_1 equation solver. The first one solves the generalized adjoint neutron transport equation using the method of characteristics (MOC), as in the forward transport equation solver. In addition, it can directly solve the generalized adjoint equation for the DH region of HTGR fuel using the Sanchez and Pomraning method. The other one solves the generalized adjoint B_1 equation for a homogenized region. The generalized adjoint B_1 equation solver has the merit of a high computation speed because it gives the generalized adjoint flux in one homogenized region without a spatial flux distribution.

In this study, the algorithm of the generalized adjoint B_1 equation solver was applied to obtain the uncertainty of the few group cross section under critical conditions. In addition, the generalized adjoint B_1 solution was used to improve the convergence of the generalized adjoint transport equation solver. First, a simple review of the generalized adjoint B_1 equation solver implemented in the DeCART for a cross section uncertainty analysis is described below.

2.1. Review of the generalized adjoint B_1 equation

After solving the forward neutron transport equation, DeCART solves the following multi-group B_1 equation to obtain the critical spectrum, which is used to generate the homogenized few-group constants for each homogenization region:

$$\mathbf{A}\boldsymbol{\Psi} = \mathbf{F}\boldsymbol{\Psi}, \tag{1}$$

where

$$\mathbf{A} = \boldsymbol{\Sigma}_t + \mathbf{D}B^2 - \boldsymbol{\Sigma}_s$$
$$= \begin{bmatrix} \Sigma_{t1} & \cdots & 0 \\ \vdots & \ddots & \vdots \\ 0 & \cdots & \Sigma_{tG} \end{bmatrix} + \frac{1}{3}\begin{bmatrix} \alpha_1\Sigma_{t1} - \Sigma_{s11}^{(1)} & \cdots & -\Sigma_{sG1}^{(1)} \\ \vdots & \ddots & \vdots \\ -\Sigma_{s1G}^{(1)} & \cdots & \alpha_G\Sigma_{tG} - \Sigma_{sGG}^{(1)} \end{bmatrix}^{-1} B^2 - \begin{bmatrix} \Sigma_{s11}^{(0)} & \cdots & \Sigma_{s1G}^{(0)} \\ \vdots & \ddots & \vdots \\ \Sigma_{sG1}^{(0)} & \cdots & \Sigma_{sGG}^{(0)} \end{bmatrix},$$

$$\mathbf{F} = \begin{bmatrix} \chi_1\nu\Sigma_{f1} & \cdots & \chi_1\nu\Sigma_{fG} \\ \vdots & \ddots & \vdots \\ \chi_G\nu\Sigma_{f1} & \cdots & \chi_G\nu\Sigma_{fG} \end{bmatrix}, \quad \boldsymbol{\Psi} = \begin{bmatrix} \phi_1 \\ \vdots \\ \phi_G \end{bmatrix},$$

and α_g is defined in the reference [2]). In Eq. (1), the cross-sections Σ_{tg}, $\nu\Sigma_{fg}$, $\Sigma_{sgg'}^{(i)}$ are the homogenized total cross-section of group g, the homogenized fission cross-section of group g multiplied by the number of neutrons per fission, and the i^{th} moment of the homogenized scattering cross-section from group g' to group g, respectively. χ_g is the fission spectrum of group g, and $\boldsymbol{\Psi}$ is the fundamental mode scalar flux.

Therefore, the eigen-mode and generalized adjoint B_1 equations for the homogenized system can be expressed as follows:

$$\mathbf{A}^*\boldsymbol{\Psi}^* = \mathbf{F}^*\boldsymbol{\Psi}^*, \tag{2a}$$

$$\mathbf{A}^*\boldsymbol{\Gamma}^* = \mathbf{F}^*\boldsymbol{\Gamma}^* + \mathbf{S}_I^*, \tag{2b}$$

where

$$\mathbf{A}^* = \mathbf{A}^T = \boldsymbol{\Sigma}_t + \mathbf{D}^T B^2 - \boldsymbol{\Sigma}_s^T,$$

$$\mathbf{F}^* = \begin{bmatrix} \chi_1\nu\Sigma_{f1} & \cdots & \chi_G\nu\Sigma_{f1} \\ \vdots & \ddots & \vdots \\ \chi_1\nu\Sigma_{fG} & \cdots & \chi_G\nu\Sigma_{fG} \end{bmatrix}, \quad \boldsymbol{\Psi}^* = \begin{bmatrix} \phi_1^* \\ \vdots \\ \phi_G^* \end{bmatrix},$$

$$\mathbf{S}_I^* = \frac{\mathbf{H}_1}{\mathbf{H}_1\cdot\boldsymbol{\Psi}} - \frac{\mathbf{H}_2}{\mathbf{H}_2\cdot\boldsymbol{\Psi}}.$$

$\mathbf{S}_I^*$ is the generalized adjoint source vector for a general response $R = \frac{\mathbf{H}_1\cdot\boldsymbol{\Psi}}{\mathbf{H}_2\cdot\boldsymbol{\Psi}}$, where $\mathbf{H}_1$ and $\mathbf{H}_2$ are the response function vector defined by the input parameters such as multi-group cross-sections.

The generalized adjoint B_1 equation, Eq. (2b), can be solved in the same way with the generalized adjoint transport equation which is described in the reference [1]. It is noted that the solution algorithm additionally needs the decontamination procedure as follows:

$$\langle\boldsymbol{\Gamma}^*\mathbf{F}\boldsymbol{\Psi}\rangle = 0. \tag{3}$$

The generalized adjoint B_1 equation combined with the auxiliary condition can be solved iteratively as follows:

$$\boldsymbol{\Gamma}_{n+1}^* = \boldsymbol{\Gamma}_n^* - C_n\boldsymbol{\Psi}^*, \tag{4}$$

where, the correction factor for the iteration is defined as $C_n = \frac{\langle\boldsymbol{\Psi}\mathbf{F}^*\boldsymbol{\Gamma}_n^*\rangle}{\langle\boldsymbol{\Psi}\mathbf{F}^*\boldsymbol{\Psi}^*\rangle}$.

Once the generalized adjoint B_1 solution, $\boldsymbol{\Gamma}^*$, is obtained, the sensitivity coefficients can be conventionally calculated using the generalized perturbation theory.

2.2. Cross section uncertainty using the critical spectrum

DeCART utilizes the B_1 equation for a critical spectrum search. The infinite spectrum can be obtained by solving the B_1 equation,

Eq. (1), with $B^2 = 0$ and the critical spectrum can be obtained by solving the B_1 equation with a critical buckling search in which the buckling, B^2, is adjusted to make the homogenized system critical. Thus, the generalized adjoint B_1 equation described in the previous section can be directly used to obtain the uncertainty critical-spectrum-weighted cross section.

To obtain the generalized adjoint flux under a critical condition, the eigen-mode forward flux and adjoint flux should be calculated in advance using the critical buckling search algorithm of the B_1 equation solver. After obtaining the forward neutron transport solution by the MOC solver, the cross-sections are homogenized by averaging the flat-source-region-wise cross-sections with a forward flux weighting and the B_1 equation, the adjoint B_1 equation, and the generalized adjoint B_1 equation are set up. The eigen-mode forward critical spectrum, adjoint critical spectrum, and B^2 for the critical system can be, then, calculated with the critical buckling search algorithm. Finally, the generalized adjoint B_1 equation, Eq. (2b), with the given critical buckling and the eigen-mode solutions can be solved as described in section 2.1. Using the generalized adjoint flux, MUSAD can calculate the sensitivities and uncertainties of the few-group cross sections for a critical system. Fig. 1 shows the algorithm for few-group cross section uncertainty analysis under critical conditions as described above.

To evaluate the uncertainty of a critical system using the generalized adjoint B_1 equation solver, the HTGR fuel pin problem, the MHTGR-350 Ex. I-1b HFP case [12], was chosen. It has a DH fuel compact which contains explicit TRISO particles with uranium oxycarbide ($UC_{0.5}O_{1.5}$) kernel randomly dispersed in a graphite matrix shown in Fig. 2. All numerical tests were performed using a 190-group cross section library and the covariance data from ENDF/B-VII.1. It is noted that the covariance data of ^{235}U ν value in ENDF/B-VII.1 are very different from those in the SCALE 44-group library.

Fig. 3 shows a comparison of the two generalized adjoint fluxes under the infinite and critical spectrum. It was observed that there are slight differences between the two solutions over the entire energy region. Table 1 shows the comparison of the k_{eff} uncertainties by the transport solution under the infinite spectrum and two B_1 solutions under the infinite spectrum and the critical spectrum. The comparison between the transport and the B_1 results reveals that the B_1 equation solver can produce a similar solution. It also shows that the k_{eff} uncertainty with the critical spectrum is similar to that with the infinite spectrum except for the contribution by the graphite scattering-scattering. Although the contribution by the graphite scattering cross section largely increases in the case with the critical spectrum, the difference in the total k_{eff} uncertainty between the two cases is not considerable because of the dominant contribution by the ^{235}U ν and ^{238}U capture cross section. Table 2 shows a comparison of the ^{238}U capture cross section uncertainty under two different spectrums. It can also be observed that the contribution of the graphite scattering slightly increases. It may be attributed to the difference of the generalized adjoint flux in the thermal range shown in Fig. 3. The total cross section uncertainties are, however, very close to each other.

It is clear that the changes between the infinite and critical spectra cause the slight difference in the contribution by the graphite scattering cross section, and it does not significantly affect the total uncertainty.

2.3. Improvement of the convergence for the generalized adjoint transport equation solver

DeCART uses the coarse mesh finite difference (CMFD) acceleration to reduce the number of the MOC iterations in the forward transport equation solution scheme. However because the

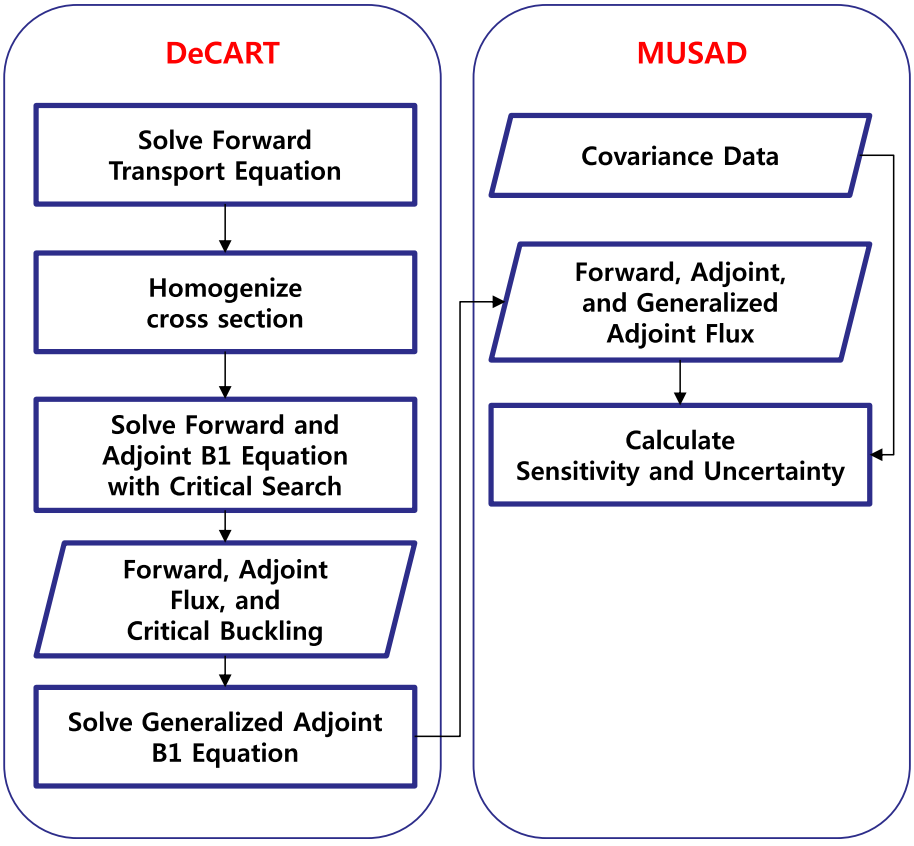

Fig. 1. Procedure for the few-group cross section uncertainty analysis under the critical condition.

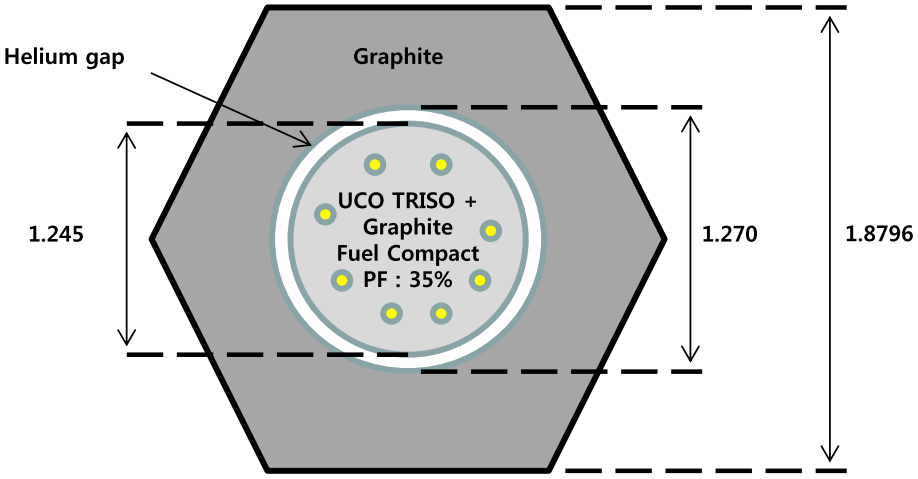

Fig. 2. Configuration of the MHTGR-350 Ex.I-1b.

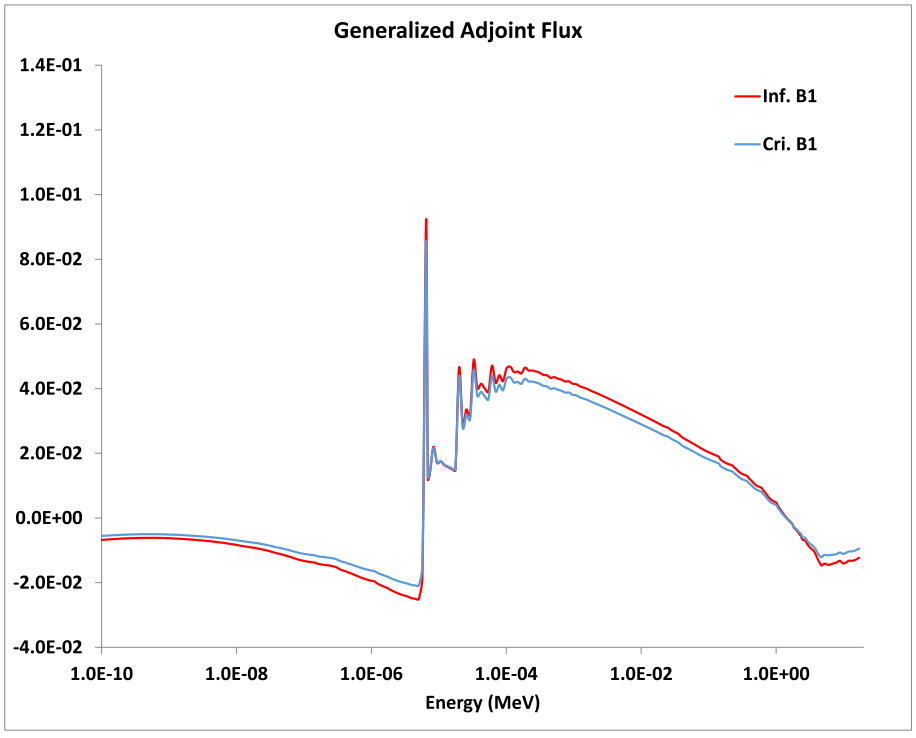

Fig. 3. Comparison of the generalized adjoint flux in the infinite and critical system.

Table 1
k_{eff} uncertainty based on the infinite and critical spectra.

Contributor	$\Delta k/k$ (%)		
	Transport (Infinite)	B1 (Infinite)	B1 (Critical)
^{235}U ν-ν	0.612	0.612	0.607
^{235}U cap-cap	0.238	0.238	0.229
^{235}U fis-cap	0.074	0.073	0.076
^{235}U fis-fis	0.071	0.071	0.082
^{238}U cap-cap	0.570	0.592	0.580
C sct-sct	**0.159**	**0.166**	**0.238**
Total	0.890	0.905	0.910

Table 2
^{238}U capture cross section uncertainty by the infinite and critical spectrum.

Contributor	$\Delta R/R$ (%)		
	Transport (Infinite)	B1 (Infinite)	B1 (Critical)
^{235}U cap-cap	0.061	0.061	0.063
^{235}U fis-cap	0.015	0.015	0.014
^{235}U fis-fis	0.026	0.026	0.024
^{238}U cap-cap	1.319	1.346	1.343
C sct-sct	**0.144**	**0.142**	**0.166**
Total	1.328	1.355	1.355

generalized adjoint equation allows negative solutions, the CMFD acceleration cannot be used for the MOC in the generalized adjoint transport equation solver. Thus, its solution should be obtained by MOC-only iterations.

To reduce the number of MOC iterations of the generalized adjoint equation solver, the generalized adjoint B_1 solution can be used as the initial value for the generalized adjoint transport solution. Before solving the generalized adjoint transport equation, the generalized adjoint B_1 solution which does not have a spatial dependency, can be quickly obtained within a few seconds.

To verify the proposed method, two different problems, Ex.I-2a fresh fuel block and Ex.I-2b burnt fuel block [12], were examined. The first one is composed of 210 fresh fuel pins defined in Ex.I-1b and 6 lumped burnable poisons in the six corners of the block shown in Fig. 4 and the convergence of the generalized adjoint solution for the ^{238}U capture cross section was investigated. The second one is composed of only burnt fuel pins with the same configuration of Ex.I-2a and that for the ^{235}U fission cross section was evaluated.

Table 3 shows the number of MOC iterations and the cross section uncertainties calculated with two different initial values, zero and the generalized adjoint B_1 solution, respectively. It reveals that the number of MOC iterations in the case of the generalized adjoint B_1 solution as the initial value decreases to 50% in both problems.

3. Implicit uncertainty reflecting double heterogeneity

DeCART/MUSAD uses the self-shielded multi-group cross section prepared by an external code system. However, the uncertainty analysis with the shielded cross section causes an inconsistency with the covariance data of the evaluated nuclear data files based on the infinitely-diluted cross sections. Thus, the uncertainty change caused by the resonance treatment should be considered as the implicit uncertainty.

In DeCART/MUSAD, the implicit uncertainty can be calculated using the Chiba method [13] based on the self-shielding factor. The method has an advantage that the implicit effect can be easily calculated in the lattice code without any data from a resonance treatment code. However, it was found that the error of the uncertainty in the DH problem of a HTGR is slightly larger than that in the homogeneous case when applying the correction method. Thus it needs an additional correction to reflect the self-shielding effect by the DH.

First, the modified correction method without the self-shielding factor is described in detail, because DeCART does not use the self-shielding factor. Then, the additional correction factor for the implicit uncertainty reflecting the DH is proposed in the next section.

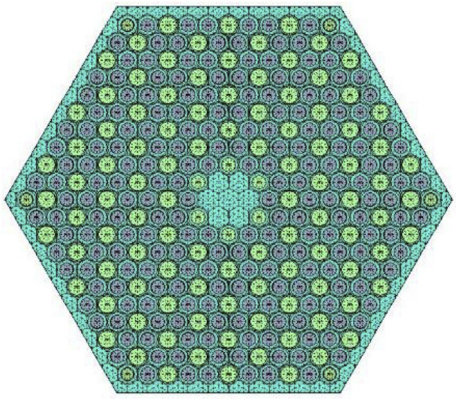

Fig. 4. Fuel block configuration of Ex.I-2a and Ex.I-2b.

Table 3
Number of MOC iterations for the generalized adjoint transport solution.

Initial Value	Ex.I-2a Fresh Fuel Block		Ex.I-2b Burnt Fuel Block	
	No. MOC Iterations (#)	^{238}U Capture XS Uncertainty (%)	No. MOC Iterations (#)	^{235}U Fission XS Uncertainty (%)
0.0 (Ref.)	17	1.351	19	0.625
B_1 Solution	9	1.351	9	0.625

3.1. The modified correction method for the implicit uncertainty

If the sensitivity of a general response, R, by an infinitely diluted cross section, σ, is expressed with the self-shielded cross section, $\tilde{\sigma}$, and the background cross section, σ_b, it can be rewritten as follows:

$$S = \frac{dR}{d\sigma}\frac{\sigma}{R} = \left(\frac{dR}{d\tilde{\sigma}}\frac{\tilde{\sigma}}{R}\right)\left(\frac{d\tilde{\sigma}}{d\sigma}\frac{\sigma}{\tilde{\sigma}}\right) = \tilde{S}\left(\frac{d\tilde{\sigma}}{d\sigma}\frac{\sigma}{\tilde{\sigma}}\right) = \tilde{S}\left(\frac{d\tilde{\sigma}}{d\sigma_b}\frac{\sigma_b}{\tilde{\sigma}}\right)\left(\frac{d\sigma_b}{d\sigma}\frac{\sigma}{\sigma_b}\right), \tag{5}$$

where, $\tilde{S}$ is the explicit sensitivity for the general response by the self-shielded multi-group cross section. Contrary to the Chiba's derivation, the resonance integral instead of the self-shielding factor can be used to obtain the relation between σ and $\tilde{\sigma}$ as follows:

$$\tilde{\sigma} = \frac{\sigma\sigma_b T}{\sigma_b - \sigma_a T}, \tag{6}$$

where, σ_a is the absorption cross section. In addition, the resonance integral, T, for the self-shielded cross section can be reproduced from Segev's interpolation [14] in DeCART as follows:

$$T = \left(\frac{\sigma_b}{\sigma_b + \eta}\right)^p, \tag{7}$$

where, η and p are the coefficients determined from the two resonance integral table entries. If applying the differentiation in terms of σ_b, Eq. (7) can be transformed as

$$\frac{dT}{d\sigma_b} = \frac{p\eta T}{\sigma_b(\sigma_b + \eta)} \tag{8}$$

Then, $\frac{d\tilde{\sigma}}{d\sigma_b}$ in Eq. (5) can be readily replaced with T from Eq. (6), Eq. (7), and Eq. (8) and the sensitivity can be approximated as follows:

$$\tilde{S}\left(\frac{d\tilde{\sigma}}{d\sigma}\frac{\sigma}{\tilde{\sigma}}\right) \cong \tilde{S}\frac{\tilde{\sigma}}{T\sigma}\left[1 - \frac{p\eta}{\sigma_b + \eta} + \frac{T\sigma}{\sigma_b}\right] = \tilde{S}\omega_1, \tag{9}$$

where, the approximation, $\frac{d\sigma_b}{d\sigma} \cong -\frac{\sigma_b}{\sigma_a}$, derived by Chiba was used for the simplification and ω_1 is the correction factor for the implicit sensitivity induced by the resonance self-shielding effect.

3.2. Implicit uncertainty correction reflecting double heterogeneity

However, it was found that the DH fuel of a HTGR has another spatial self-shielding effect. It means that the uncertainty is changed by the DH effect and it needs an additional correction.

We can define the relation between the effective cross section for the DH region, $\hat{\sigma}$, and the multi-group cross section, $\tilde{\sigma}$, as follows:

$$\hat{\sigma} = \gamma\tilde{\sigma}, \tag{10}$$

where, γ is the self-shielding factor for the DH.

Because DeCART adopts the renewal theory by Sanchez and Pomraning, the self-shielding factor for the DH can be approximated as follows:

$$\gamma \approx \frac{\hat{\Sigma}}{\Sigma_{mix}}, \tag{11}$$

where, $\hat{\Sigma}$ is the macroscopic effective cross section for the DH region approximated by the renewal theory. The detailed explanation for the effective cross section can be found in the reference [9]. In addition, Σ_{mix} is the volume weighted cross section for the mixture with the TRISO fuel as follows:

$$\Sigma_{mix} = p_0\Sigma_0 + \sum_{ik} p_{ik}\Sigma_{ik}, \tag{12}$$

where, p_0 and Σ_0 are the volume fraction and the total cross section for the base material of the fuel compact and p_{ik} and Σ_{ik} are the volume fraction and the total cross section for the k-th layer of the i type TRISO.

One can derive the sensitivity considering the self-shielding effect of the DH as follows:

$$S = \left(\frac{dR}{d\tilde{\sigma}}\frac{\hat{\sigma}}{R}\right)\left(\frac{d\hat{\sigma}}{d\tilde{\sigma}}\frac{\tilde{\sigma}}{\hat{\sigma}}\right)\left(\frac{d\tilde{\sigma}}{d\sigma}\frac{\sigma}{\tilde{\sigma}}\right) = \hat{S}\left(\frac{d\hat{\sigma}}{d\tilde{\sigma}}\frac{\tilde{\sigma}}{\hat{\sigma}}\right)\left(\frac{d\tilde{\sigma}}{d\sigma}\frac{\sigma}{\tilde{\sigma}}\right) \approx \hat{S}\left(\frac{d\gamma}{d\tilde{\sigma}}\frac{\tilde{\sigma}}{\gamma}+1\right)\omega_1 = \hat{S}\omega_2\omega_1, \tag{13}$$

where, $\hat{S}$ is the sensitivity by the effective cross section and $\frac{d\hat{\sigma}}{d\tilde{\sigma}}$ can be rewritten with the perturbation equation to Eq. (10). In addition, ω_1 is defined in Eq. (9) and ω_2 is the correction factor for the implicit sensitivity of the DH. The correction factor can be calculated by the direct perturbation as follows:

$$\frac{d\gamma}{d\tilde{\sigma}}\frac{\tilde{\sigma}}{\gamma}+1 \approx \frac{\Delta\gamma}{\Delta\tilde{\sigma}}\frac{\tilde{\sigma}}{\gamma}+1 \tag{14}$$

The verification calculation of the proposed correction method was performed with the MHTGR 350 Ex.I-1b CZP and HZP problems shown in Fig. 2. The reference results were obtained from McCARD [15] based on the Monte Carlo method.

Table 4 shows the comparisons between the reference and the explicit and implicit uncertainty by MUSAD for the problems. The explicit uncertainty caused by the ^{238}U absorption-absorption in the MUSAD result was overestimated to about 40% compared with the McCARD result. On the other hand, in the case when considering the implicit uncertainty by the resonance self-shielding effect, the differences from the reference decrease to about 4% in the CZP case and 11% in the HFP case, respectively. Moreover, when applying the implicit effect correction by the DH, the difference in the HFP case decreases to 2.3%. Considering the simple correction without any data from the external resonance treatment code as shown in Eq. (13), it is clear that the proposed method is considerably effective.

4. HTGR UAM benchmark results

In our previous study [6], we established a two-step procedure for an uncertainty analysis of the HTGR core parameters. The DeCART/MUSAD code system was used in the lattice step to calculate few-group cross section uncertainty and to generate the random sampled few-group cross section sets. A core simulation code for HTGR, CAPP, was then applied to generate the core parameters with the sampled few-group cross section sets and the uncertainty for them can be simply obtained by statistical processing.

The DeCART/MUSAD code was improved by the methods described in previous sections. The generalized adjoint solutions were obtained using the generalized adjoint transport equation with the initial value from the generalized adjoint B1 equation and the implicit uncertainties were corrected by the correction factor to reflect the resonance self-shielding effect and DH effect. The performance of the code system was examined with the MHTGR-350 Ex.II-2 3D core benchmark. It consists of two problems, Ex.II-2a and Ex.II-2b. The first one consists of the fresh fuel and the reflector blocks and the second consists of the fresh fuel, the burnt fuel, and the reflector blocks. It is noted that the two core problems involve the steady-state neutronics calculation at the HFP condition without any temperature feedback. The calculation results are provided in the next two sections.

4.1. MHTGR-350 Ex. II-2a benchmark

MHTGR-350 Ex. II-2a consists of the fresh fuel blocks of Ex.I-2a shown in Fig. 4 and the graphite reflector blocks. Fig. 5a shows the radial configuration of the core. The 3D core has axially 4 bottom reflector layers, 10 identical fuel layers, and 2 top reflector layers.

First, DeCART/MUSAD generated the few-group cross section and their uncertainties for the fresh fuel block using the super cell as shown in Fig. 5b, and the reflector cross section using the super cell shown in Fig. 5c. In addition, MUSAD generated the random

Table 4
k_{inf} uncertainty for Ex.I-1b.

Problem	Ex.I-1b CZP				Ex.I-1b HFP			
Code	McCARD	DeCART/MUSAD			McCARD	DeCART/MUSAD		
Contributor	Type							
	Explicit+ Implicit (%)	Explicit (%)	Explicit+ Implicit1 (%)	Explicit + Implicit2 (%)	Explicit+ Implicit (%)	Explicit (%)	Explicit + Implicit1 (%)	Explicit + Implicit2 (%)
^{235}U ν-ν	0.617	0.617	0.617	0.617	0.611	0.612	0.612	0.612
^{235}U abs-abs	0.239	0.240	0.239	0.239	0.237	0.238	0.238	0.237
^{235}U fis-fis	0.065	0.065	0.065	0.065	0.071	0.071	0.071	0.071
^{238}U abs-abs	**0.316**	**0.437**	**0.328**	**0.312**	**0.388**	**0.555**	**0.432**	**0.397**
Total	0.753	0.815	0.762	0.755	0.784	0.883	0.811	0.793

Implicit1: Implicit uncertainty by resonance self-shielding effect.
Implicit2: Implicit uncertainty by resonance self-shielding effect and double heterogeneity.

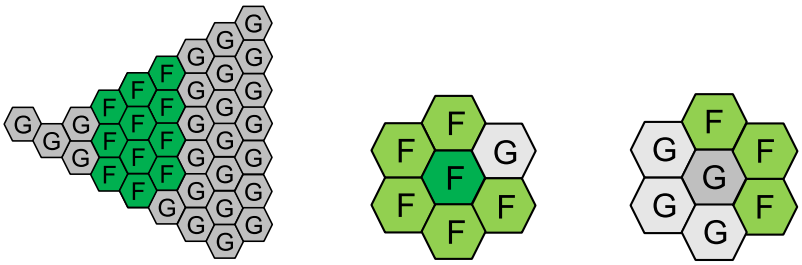

(a) Ex.II-2a core (b) Super cell for the fresh fuel block (c) Super cell for the reflector

Fig. 5. Ex.II-2a core layout and the super cell configuration.

Table 5
Core parameter uncertainties for Ex.II-2a.

Problem	3D Core		Super Cell for Fresh Fuel Block
Code	DeCART/MUSAD/CAPP		DeCART/MUSAD
Parameter	k_{eff}	Axial Offset (%)	k_{inf}
Value	1.05994	−0.012	1.08757
Uncertainty (%)	0.731	4.516	0.747

sampled few-group cross section sets based on their uncertainties. The number of few-group cross section sets is 600 in this study. In the second step, CAPP performed the 3D core analysis with the sampled few-group cross section sets.

Table 5 shows the k_{eff} uncertainty for the 3D core problem. For the comparison, it also shows the k_{inf} uncertainty of the super cell problem for the fresh fuel block cross section shown in Fig. 5b. Because the Ex.II-2a core consists of only the fresh fuel block, the k_{eff} uncertainty for the core is similar to that of the super cell problem. In addition, the table shows the uncertainty for the axial offset of the 3D core. It is relatively a large value due to the very small axial offset. Fig. 6 shows the relative radial power distribution and their uncertainties. The uncertainties for the relative radial power are very small, because the core consists of only one fuel block type. Of note, there have been no reference results for Ex.II-2 reported by the HTGR UAM yet.

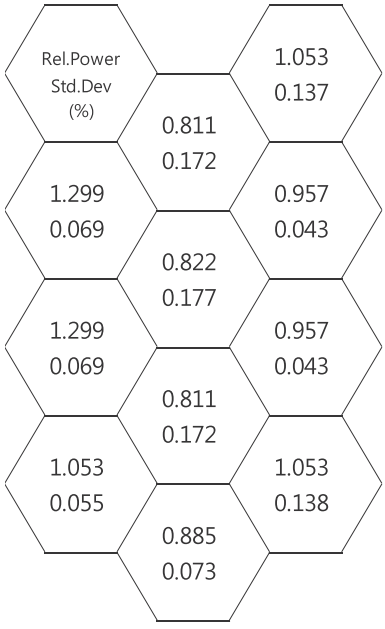

Fig. 6. Radial power distribution and their uncertainty for Ex.II-2a.

4.2. MHTGR-350 Ex. II-2b benchmark

MHTGR-350 Ex. II-2b consists of the fresh fuel blocks, the burnt fuel blocks, and the graphite reflector blocks shown in Fig. 7. It has a reflector block with a control rod partially inserted in position C shown in Fig. 7a. The figure also shows the super cell models for generating the few-group cross sections of the fresh fuel block, the burnt fuel block, and the graphite block, respectively.

Table 6 presents the uncertainties for the k_{eff} and the axial offset of the core. The k_{eff} uncertainty is smaller than that of the fresh fuel block due to the burnt fuel block. The axial offset is more negative and its uncertainty is smaller due to the control rod. In addition, Fig. 8 shows the relative radial power distribution and their uncertainties for the core. They are larger than those of Ex.II-2a due to the configuration with two fuel types.

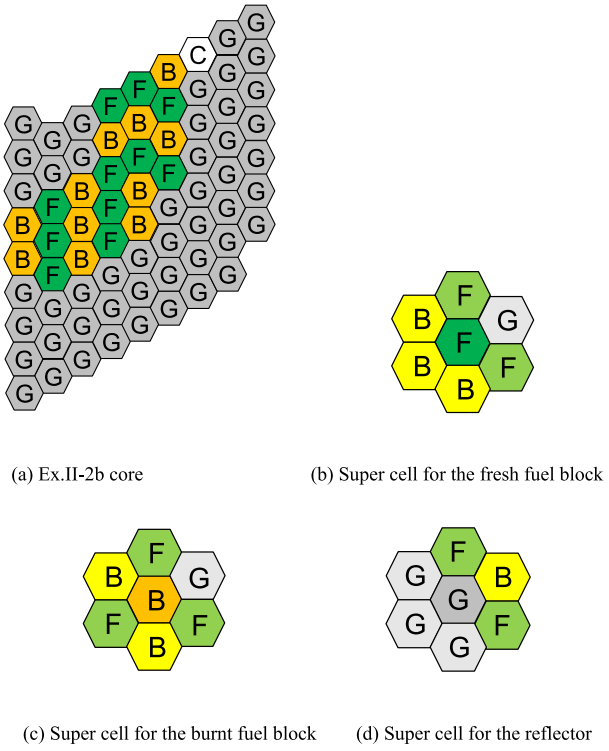

(a) Ex.II-2b core (b) Super cell for the fresh fuel block

(c) Super cell for the burnt fuel block (d) Super cell for the reflector

Fig. 7. Ex.II-2b core layout and the super cell configurations.

Table 6
Core parameter uncertainties for Ex.II-2b.

Problem	3D Core		Super Cell for Fresh Fuel Block	Super Cell for Burnt Fuel Block
Code	DeCART/MUSAD/CAPP		DeCART/MUSAD	DeCART/MUSAD
Parameter	k_{eff}	Axial Offset (%)	k_{inf}	k_{inf}
Value	1.04104	−0.108	1.05621	1.04503
Uncertainty (%)	0.695	1.529	0.776	0.581

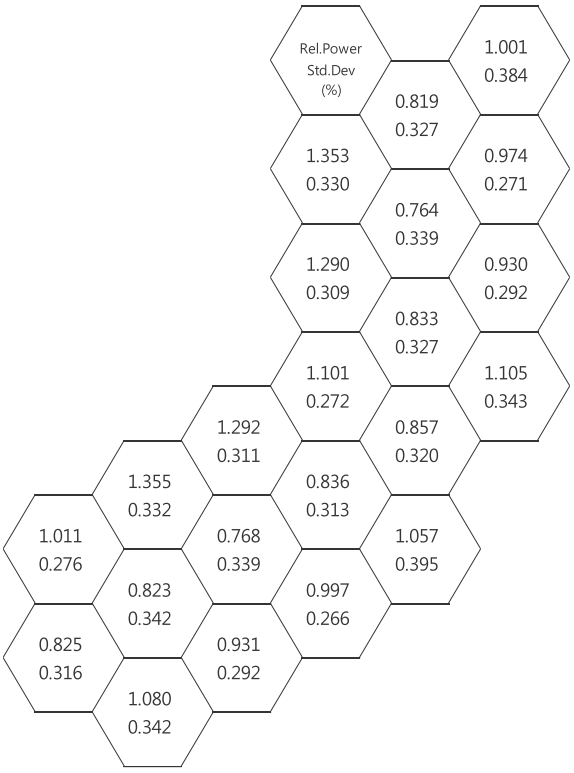

Fig. 8. Radial power distribution and their uncertainty for Ex.II-2b.

5. Conclusions

In this paper, the improvements of the DeCART/MUSAD code system for the uncertainty analysis of the HTGR neutronic parameters were presented. The function for quantifying an uncertainty of the critical-spectrum-weighted few group cross section was implemented using the generalized adjoint B_1 equation solver. First, the eigen-mode forward critical spectrum and adjoint critical spectrum were calculated with the critical buckling search algorithm. Then, the generalized adjoint B_1 equation with the given critical buckling was solved. Though the changes between the infinite and critical spectra caused a considerable difference in the contribution by the graphite scattering cross section, it does not significantly affect the total k_{eff} uncertainty. In addition, to reduce the number of MOC iterations of the generalized adjoint equation solver, the generalized adjoint B_1 solution was used as the initial value for the generalized adjoint transport solution. The number of MOC iterations in that case decreased to 50% compared with the case of the zero initial values. To reflect the implicit uncertainty by the self-shielding effect in the DeCART/MUSAD, the modified correction factor without the self-shielding factor was derived with the resonance integral. It reduced the differences from the reference in the uncertainty induced by the ^{238}U absorption cross section from 40% to 4% in the CZP case and 11% in the HFP case. Moreover, the additional correction factor for the implicit uncertainty reflecting the DH was proposed in this paper. It was expressed in terms of the effective cross section proposed by Sanchez and Pomraning and it reduced the error in the contribution by the ^{238}U absorption cross section to 2.3%.

The DeCART/MUSAD code was improved by the proposed methods and its performance was examined with the MHTGR-350 Ex.II-2 3D core benchmark. In the case of Ex.II-2a core composed of the fresh fuel blocks only, the k_{eff} uncertainty for the core was very similar to that of the super cell problem for the fresh fuel block cross section. In addition, the k_{eff} uncertainty for Ex.II-2b which consists of fresh fuel blocks and burnt fuel blocks was smaller than that of the fresh fuel block.

Acknowledgements

This work was supported by the National Research Foundation of Korea (NRF) grant funded by the Korea government (MSIP) (No. 2017M2A8A1014757).

References

[1] T.Y. Han, et al., Development of a sensitivity and uncertainty analysis code for high temperature gas-cooled reactor physics based on the generalized perturbation theory, Ann. Nucl. Energy 85 (2015) 501–511.
[2] T.Y. Han, et al., Uncertainty analysis with double heterogeneity treatment based on the generalized perturbation theory, Ann. Nucl. Energy 106 (2017a) 111–117.
[3] R.L. Childs, Generalized Perturbation Theory Using Two-Dimensional, Discrete Ordinates Transport Theory, Oak Ridge National Laboratory, 1980. ORNL/CSD/TM-127.
[4] Yigal Ronen, CRC Handbook of Nuclear Reactors Calculations, vol. III, CRC Press, 1986.
[5] A. Yankov, et al., A Two-step Approach to Uncertainty Quantification of Core Simulators, Science and Technology of Nuclear Installations, 2012, 2012.
[6] T.Y. Han, et al., Development of Two-step Procedure for Uncertainty Analysis of VHTR Core Parameters, vol. 117, Transaction of American Nuclear Society, 2017b, pp. 808–810.
[7] J.Y. Cho, et al., Improvement and verification of the DeCART code for HTGR core physics analysis, Nucl. Eng. Technol. 51 (2019) 13–30.
[8] H.C. Lee, et al., Development of HELIOS/CAPP Code System for the Analysis of Block Type VHTR Cores, PHYSOR 2012, Knoxville, Tennessee, 2012. April 15-20.
[9] R. Sanchez, G.C. Pomraning, A statistical analysis of the double heterogeneity problem, Ann. Nucl. Energy 18 (7) (1991) 371–395, 1991.
[10] L. Pogosbekyan, et al., Resolution of Double Heterogeneity in Direct Transport Calculation Employing Subgroup Method and Method of Characteristics, PHYSOR 2008, Switzerland, 2008.
[11] G. Strydom, et al., IAEA Coordinated Research Project on HTGR Physics, Thermal-Hydraulics, and Depletion Uncertainty Analysis - Prismatic HTGR Benchmark Specification: Phase II, Idaho National Laboratory, 2018. INL/EXT-18-44815, Rev. 0, April, 2018.
[12] G. Strydom, et al., IAEA Coordinated Research Project on HTGR Physics, Thermal-Hydraulics, and Depletion Uncertainty Analysis - Prismatic HTGR Benchmark Definition: Phase I, Idaho National Laboratory, 2015. INL/EXT-15-34868, Rev. 1, Sep, 2015.
[13] G. Chiba, et al., Resonance self-shielding effect in uncertainty quantification of fission reactor neutronics parameters, Nucl. Eng. Technol. 40 (2014) 281–290.
[14] M. Segev, Interpolation of resonance integrals, Nucl. Sci. Eng. 17 (1981) 113–118.
[15] H.J. Shim, et al., Adjoint sensitivity and uncertainty analyses in Monte Carlo forward calculations, J. Nucl. Sci. Technol. 48 (12) (2012) 1453–1461.